J. Fluid Mech. (2002), *vol.* 467, *pp.* 41–56.
DOI: 10.1017/S002211200200157X Printed in the United Kingdom

Particle image velocimetry investigation of a turbulent boundary layer manipulated by spanwise wall oscillations

By GAETANO MARIA DI CICCA[1], GAETANO IUSO[1], PIER GIORGIO SPAZZINI[2] AND MICHELE ONORATO[1]

[1]Dipartimento di Ingegneria Aeronautica e Spaziale, Politecnico di Torino, C.so Duca degli Abruzzi, 24, I 10129 Torino, Italy

[2]CNR-CSDF c/o Dipartimento di Ingegneria Aeronautica e Spaziale, Politecnico di Torino, C.so Duca degli Abruzzi, 24, I 10129 Torino, Italy

(Received 22 October 2001 and in revised form 26 April 2002)

Particle image velocimetry has been applied to the study of a canonical turbulent boundary layer and to a turbulent boundary layer forced by transversal wall oscillations. This work is part of the research programme at the Politecnico di Torino aerodynamic laboratory with the objective of investigating the response of near-wall turbulence to external perturbations. Results are presented for the optimum oscillation period of 100 viscous time units and for an oscillation amplitude of 320 viscous units. As expected, turbulent velocity fluctuations are considerably reduced by the wall oscillations. Particle image velocimetry has allowed comparisons between the canonical and forced flows in an attempt to find the physical mechanisms by which the wall oscillation influences the near-wall organized motions.

1. Introduction

It is well accepted (Robinson 1991; Panton 1997) that in a turbulent boundary layer the dominant organized (coherent) motions, in the region where the rate of turbulence energy production exceeds dissipation (approximately up to $y^+ = 100$; here $+$ is used for quantities normalized with respect to viscous units), are trains of quasi-longitudinal vortical structures and quasi-streamwise velocity streaks. It has also long been recognized that vortical motions cause the velocity streaks by advecting the mean momentum gradient (see e.g. Blackwelder & Eckelmann 1979) and that several vortical structures are associated with each streak (see e.g. Jimenez & Moin 1991), but the physical process leading to the creation of new vortical structures is not yet understood to a satisfactory degree. Most of the numerous proposed regeneration mechanisms involve the generation of new vortical structures either by induction from existing vortices or by local instability of the velocity streaks (Panton 1997).

A powerful experimental technique for investigating the physics of near-wall turbulence is to study its response to external perturbations. Following this idea, a research programme on near-wall turbulence control was started at our laboratory, dealing with different forcing flows, such as the ones generated by outer-layer devices (Iuso & Onorato 1995), by large-scale longitudinal embedded vortices (Di Cicca *et al.* 1999; Onorato *et al.* 2000; Iuso *et al.* 2002) and by spanwise wall oscillations. The present paper deals with a flat plate turbulent boundary layer forced by spanwise

oscillations of the wall. The resulting flow is compared with the standard boundary layer flow, with emphasis on the behaviour of the experimentally detected organized motions in an attempt to interpret the observed differences between the natural and the manipulated flows in terms of proposed regeneration mechanisms for near-wall turbulent energy.

Turbulent boundary layer control by means of spanwise wall oscillations is not a new research subject; indeed it is well known that appropriate three-dimensional disturbances introduced into the flow produce friction drag and turbulence reductions. The cause of these reductions is not yet completely understood.

Jung, Mangiavacchi & Akhavan (1992) conducted a DNS study ($Re_h = 3000$) of a turbulent channel flow subject either to an oscillatory spanwise cross-flow or to spanwise oscillatory motions of one of the channel walls. Their results indicate a 40% reduction in friction drag when the non-dimensional period of oscillation T^+ was set to 100. The oscillations also gave rise to a 40% reduction in the streamwise component of the Reynolds stress, with no significant increase in the spanwise component. These friction drag and turbulence reduction results were experimentally confirmed by Laadhari, Skandaji & Morel (1994) for a boundary layer flow at $Re_\theta = 950$. In that paper it was conjectured that the continuous shifting of the longitudinal vortices to different positions relative to the wall velocity streaks weakens the intensity of the streaks, by injecting high-speed fluid into low-speed streaks and low-speed fluid into high-speed regions. The effect of the wall-oscillation amplitude on the total energy balance was investigated by Baron & Quadrio (1996) using DNS. For an oscillation period of $T^+ = 100$ they found a 10% net energy saving with a spanwise wall velocity oscillation amplitude of $Q_x/8h$, where Q_x is the streamwise flow rate per unit width for the unperturbed flow and h is the channel half-height. An experimental investigation into changes in the turbulent boundary layer structure with spanwise wall oscillations was carried out by Choi, DeBisschop & Clayton (1998) and Choi (2000). In agreement with previously mentioned DNS and laboratory experiments a reduction of 45% in the skin friction coefficient was measured with wall oscillations. Choi *et al.* (1998) and Choi (2000) related the mechanism of drag reduction by spanwise wall oscillations to the spanwise vorticity generated by the periodic Stokes layer over the oscillating wall. Dhanak & Si (1999) were able to demonstrate numerically that the interaction between evolving, axially stretched, streamwise vortices and a Stokes layer on the oscillating surface beneath them leads to reductions in skin friction.

All previously reported research on turbulence manipulation by spanwise wall motion were conducted via numerical simulation or via physical experiments, in which data were taken by pointwise measurements, hot wires or laser Doppler velocimetry. In the present work measurements are made using digital particle image velocimetry, which allows the direct observation of the near-wall organized motions or of their signature.

2. Experiments

Experiments were carried out in the Hydra water tunnel. This facility is a closed-loop, open-surface channel with a 350 mm × 500 mm × 1800 mm test section. Measurements were taken on a horizontal flat plate positioned in the test chamber. The sinusoidal oscillation of the plate spans the whole test section from wall to wall, and was produced by a crank-shaft system with an operating frequency in the range from 0 to 5 Hz. The results presented here refer to a wall oscillation frequency of 2.67 Hz, corresponding to a period of 100 viscous units, $T^+ = 100$. The peak-to-peak ampli-

tude of the moving wall was 2 cm, corresponding to 324 viscous units, $\Delta z^+ = 324$. Viscous units are here referred to the case of the standard (i.e. in absence of wall oscillation) boundary layer.

The water of the tunnel was seeded with spherical solid particles of 2 μm nominal diameter. A Nd-YAG laser source with 200 mJ of energy per pulse and a duration of 8 ns provided double-pulsed light sheets (approximately 0.5 mm thick) with a repetition rate of 10 Hz. Images were recorded using a 1008×1012 pixels CCD videocamera (Kodak Megaplus ES 1.0).

The standard turbulent boundary layer flow was characterized by Reynolds number based on the momentum thickness $Re_\vartheta = 1160$, shape factor $H = 1.32$, ratio between the friction velocity u_τ and the external velocity U_e equal to 0.044, thickness $\delta = 43$ mm and free-stream turbulence of 1.2%.

Particle image velocimetry (PIV) measurements were taken in a plane (x, z) parallel to the wall and in a streamwise plane (x, y) normal to the wall; x is the streamwise coordinate. The (x, z) images were situated in the buffer layer at a distance of 20 viscous units from the wall, $y^+ = 20$; the images in the plane (x, y) span the buffer layer and approximately the whole logarithmic region, as y^+ ranges from 0 to 310.

The local particle image displacement was determined by using a cross-correlation-based algorithm (Adrian 1991; Willert & Gharib 1993), structured as an iterative multigrid method (Scarano & Riethmuller 1999). The image analysis started with an interrogation window of 64×64 pixels and the vector field obtained at this step was used for appropriately shifting the interrogation windows during the successive analysis at 32×32 pixels. In the last iteration the interrogation cells overlapped by 50%.

After being computed by interrogating every image couple, vector fields were validated by applying standard post-processing procedures (Di Cicca 2001). Removed velocity vectors were replaced by using a bilinear interpolation. Each vector represents a locally filtered value of the velocity in a physical dimension (Δx, Δy, Δz) corresponding respectively to ($\Delta x^+ = 17.8$, $\Delta y^+ = 8.1$, $\Delta z^+ = 17.8$) in the plane (x, z) and to ($\Delta x^+ = 10.4$, $\Delta y^+ = 10.4$, $\Delta z^+ = 8.1$) in the plane (x, y). The spatial resolution in the (x, z)-plane is then equal to about 10 Kolmogorov lengthscales, while in the (x, y)-plane, for $y^+ > 100$, it ranges (in the wall-normal direction) from 3.1 to 4.1 Kolmogorov lengthscales.

Statistical analysis was performed by averaging over 600 PIV images in both planes (x, z) and (x, y).

3. Standard boundary layer: results and comments

In this section PIV results for the instantaneous flow field in the planes (x, z) and (x, y) are shown for the case of the basic boundary layer without wall oscillation. In figure 1 the grey level map of the instantaneous streamwise fluctuating component, u, of the velocity in the plane (x, z) at $y^+ = 20$ is shown. The observed flow field covers 525 viscous lengths in both the streamwise and spanwise directions. The mean external flow comes from the left. Superimposed on the fluctuating streamwise velocity, instant signatures of vortical structures are indicated by the circular arrows. The continuous and dotted isolines represent contours of the instantaneous wall-normal component of the vorticity, ω_y. As expected, in the buffer layer region quasi-streamwise low-speed streaks characterize the flow, with a spanwise spacing of the order of 100 viscous lengths (Smith & Metzler 1983). The typical irregular wavy appearance of the streaky structures seen in theoretical models (Landahl 1990) as well as in numerical

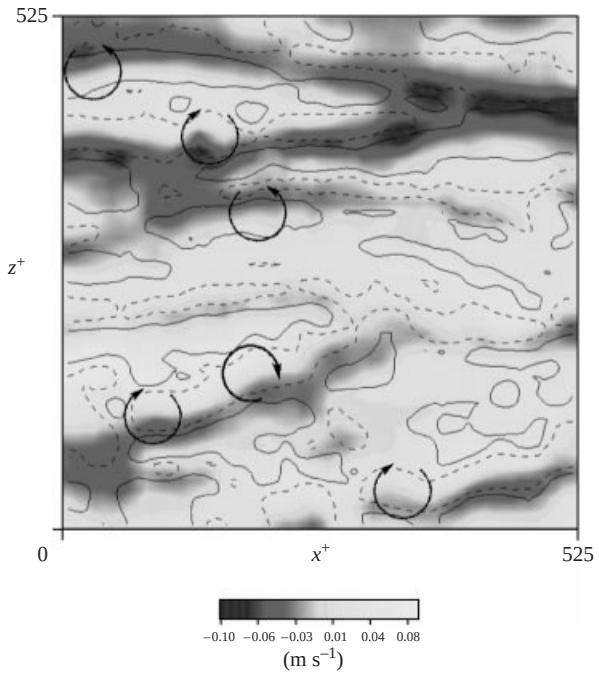

FIGURE 1. Velocity streaks, vortical motion signatures and contours of ω_y. Continuous line: $\omega_y = +15\,\mathrm{s}^{-1}$; dotted line: $\omega_y = -15\,\mathrm{s}^{-1}$; $y^+ = 20$.

simulations (Johansson, Alfredsson & Kim 1991) and in experimental results (Gottero & Onorato 2000) is evident in the present results. The importance of the meandering of the streaky velocity patterns in producing steep streamwise and spanwise gradients of the longitudinal fluctuating velocity, u, has been proved in the previously cited references. The swirling motions reported in figure 1 are the cross-sections of quasi-streamwise vortices or of legs of hairpin structures that are cut by the laser light sheet. In the present paper vortex signatures in two-dimensional planes are first identified through the method introduced by Chong *et al.* (1990), which involves the analysis of the eigenvalues corresponding to the local velocity gradient tensor. When the swirling structure is detected, validation is performed by observing the vectorial flow field after a suitable Galilean decomposition (Adrian, Christianssen & Liu 2000*a*) and the vorticity field (Di Cicca *et al.* 2001).

Vortex signatures in figure 1 and in similar images at different instants have elliptical (in some instances, almost circular) shapes and visualize vortical structures whose (vertical) inclination at that instant is large enough to display a swirling motion in the plane (x, z). The map (figure 1) shows that the vortices appear on both sides of the low-speed streaks and with different rotation directions, clockwise on the left side of the streak and counter-clockwise on the right side (looking downstream). This association of low-speed streaks with vortices is found in every realization of the present flow and is a consequence of the induced low-momentum fluid on the side of the quasi-longitudinal vortex (or of one hairpin leg), where the structure lifts up the fluid from the wall. As shown also in similar images taken at different instants, several vortical structures are associated with a single low-speed streak and in the buffer layer many vortices have an inclination angle presumably much higher than the 9° mean value forecast by the near-wall structure conceptual model of Jeong

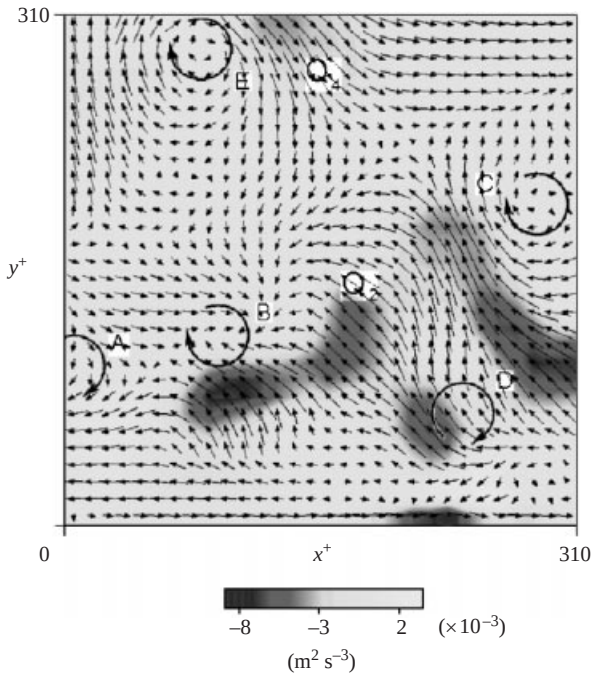

FIGURE 2. Reynolds decomposed velocity field, swirling motions, quadrant events and instantaneous contribution to turbulent kinetic energy (grey level map) in a plane (x, y).

et al. (1997). Moreover, very few pairs of counter-rotating vortices symmetrical in the spanwise direction with respect to a low-speed streak have been observed, as would be expected in the case of symmetric hairpins generating the low-speed streak between their legs. This seems to confirm what has been observed by Robinson (1993) from his DNS data of turbulent channel flow, i.e. that quasi-longitudinal vortices dominate the buffer layer region, while complete symmetric hairpin structures are rare. Figure 1 also highlights the high values of ω_y flanking the low-speed streaks. It has been demonstrated (Jimenez & Pinelli 1999; Schoppa & Hussain 2002) that such high values of ω_y, caused by the u-velocity structure, are of paramount importance for the generation of longitudinal vortices and for the subsequent maintenance of the turbulence.

Figure 2 represents the instantaneous flow field in the streamwise plane (x, y), normal to the wall, at the symmetry centreline of the flat plate. The images cover 310 by 310 viscous lengths; the mean velocity direction is from the left to the right. The instantaneous velocity field is dominated by the dynamics of vortical structures. Quasi-longitudinal vortical structures may be detected if they tilt (in the horizontal plane) far enough to capture their swirling motion in the plane (x, y). In particular, a vortex has to be tilted by an angle much larger than the mean tilting angle of $\pm 4^\circ$ claimed by Jeong *et al.* (1997) in their conceptual model of near-wall structure in order to be seen in the plane (x, y). Hairpin-shaped vortices, on the other hand, are expected to be easily detected in the plane (x, y) when the image plane cuts their heads. Five vortical structures indicated as A, B, C, D, E are clearly identified. The swirling patterns A, B and C are aligned in a direction forming an angle of about $+15^\circ$ with respect to the wall in the streamwise direction. The correspondence between the vortical structure organization observed in figure 2 and the results of Adrian and co-workers is evident.

They detected aligned hairpin packets growing upwards in the streamwise direction at a mean angle of approximately $+12^\circ$ both in DNS results (Zhou *et al.* 1999) and PIV measurements (Adrian, Meinhart & Tomkins 2000*b*). Vortex D, in the lower part of the boundary layer, is also consistent with the regeneration mechanisms described by Zhou *et al.* (1999). Vortex E may be the signature of a hairpin developing upstream. Similar configurations have been found in several other realizations. Moreover, by associating this result with what has been shown in planes parallel to the wall (at $y^+ = 20$), namely that vortex couples exhibiting symmetrical behaviour with respect to a low-speed streak are rare, it may be inferred that hairpin structures are most frequently not completely formed, i.e. they do not have symmetrical legs but consist of simple arch vortices. This is consistent with the definition of hairpin structure given in Adrian *et al.* (2000*b*), namely: "The term hairpin is here taken to represent cane, hairpin, horse-shoe or omega-shaped vortices and deformed versions …". Furthermore observe in figure 2 how not all the detected vortex signatures are shown by the Reynolds decomposed velocity field. Note that these vortices are clearly visible when the flow field is decomposed by subtracting locally a constant velocity nearly corresponding to the vortex convection velocity (Adrian *et al.* 2000*a*). Important flow features follow from the vortex organization described in figure 2 and from the Reynolds decomposed flow field. A low-speed streak generated by the hairpin packet is evident in the near-wall region, where reverse flow is present. Below the signatures of the swirling structures, and in particular for vortices B and C, a strong ejection of low-momentum fluid is present as a result of the collective pumping effect from the hairpin legs and heads in the packet. These ejections of low-momentum fluid represent Q2 (second quadrant) motions whose occurrence and frequency have been the subject of several experimental studies. Planar PIV measurements offer the opportunity of directly observing and understanding these motions in conjunction with the causes determining their behaviour. The low-momentum fluid (Q2 event) meets the high-momentum fluid (Q4 event) from the outer region, forming internal shear layers. The grey level map in figure 2 represents the quantity $(uv)\,\mathrm{d}U/\mathrm{d}y$ whose negative counterpart is the instant contribution to the production term in the turbulent kinetic energy equation. It can be seen that the main contribution to the turbulence production comes from Q2 events below $y^+ = 100$ and that Q4 events do not provide significant production.

4. Oscillating wall: results and comments

Instantaneous maps corresponding to the ones presented in the previous section show that the organization of the flow, for the case of the oscillating wall, is qualitatively similar to that for the standard boundary layer. No appreciable differences can be estimated by visual inspection of them. Hence in this section comparison between the basic and the forced flows will be essentially based on statistical analysis.

Mean velocity profiles are first displayed in the log-law plot of figure 3; the manipulated velocity profiles were normalized using the friction velocities of both the canonical and forced cases. Wall-shear stress was evaluated by means of the near-wall slope of the mean velocity profile and was confirmed by the fact that the mean velocity U at the first measurement points in the viscous sublayer, when normalized with respect to the estimated value of the friction velocity, satisfies the expected relation $U^+ = y^+$ (Choi *et al.* 1998). The marked upward shifting of the logarithmic velocity profile for the forced flow, when actual inner-scaling (i.e. performed with the inner variables corresponding to the case being discussed) is applied, confirms that

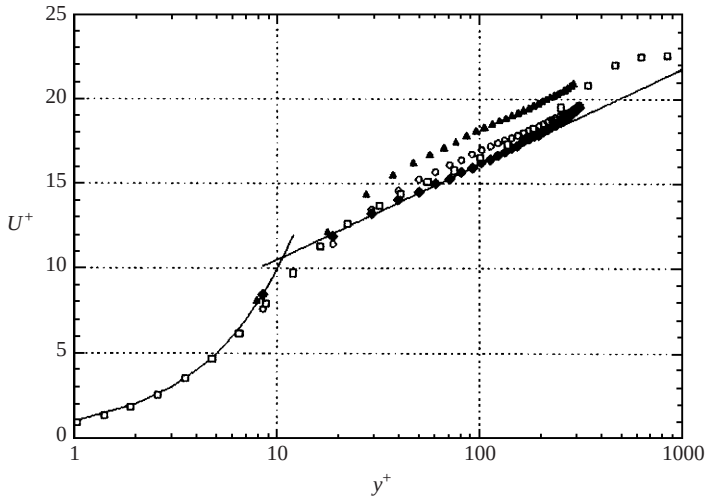

FIGURE 3. Log-law plot of mean velocity profiles. Solid line: law of the wall; solid diamond: standard boundary layer; open circles: manipulated boundary layer (u_τ standard boundary layer); solid triangle: manipulated boundary layer (actual u_τ); open square: LDV data from De Graaf & Eaton (2000) for a standard boundary layer.

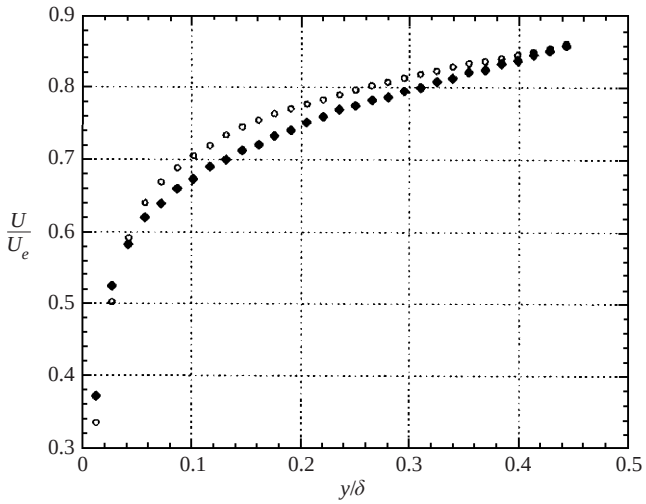

FIGURE 4. Mean velocity profiles. Solid diamond: standard boundary layer; open circle: manipulated boundary layer.

the skin-friction drag is reduced by spanwise wall oscillation. This is typical of most drag-reducing flows and suggests the thickening of the viscous sublayer. The increase in depth of the viscous sublayer reflects a reorganization of the turbulent structures, including an increase in the smallest eddies scale and a displacement of turbulent events outwards from the wall (Choi *et al.* 1998). When quantities are normalized with respect to the friction velocity of the standard boundary layer, figure 3, or more clearly when they are outer-scaled in linear coordinates, figure 4, a reduction of the mean velocity is observed throughout the region $y^+ < 30$ ($y/\delta < 0.04$). Further from the wall the mean velocity is slightly larger in order to conserve momentum.

Velocity fluctuation results are compared in figure 5, where considerably large

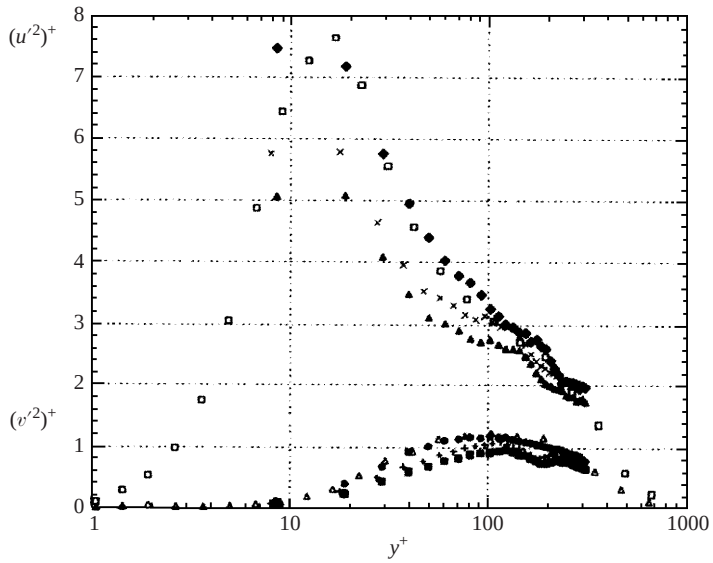

FIGURE 5. Profiles of velocity component variance. Solid diamond: $(u'^2)^+$ standard boundary layer; solid triangle: $(u'^2)^+$ manipulated boundary layer (u_τ standard boundary layer); cross: $(u'^2)^+$ manipulated boundary layer (actual u_τ); solid circle: $(v'^2)^+$ standard boundary layer; solid square: $(v'^2)^+$ manipulated boundary layer (u_τ standard boundary layer); plus: $(v'^2)^+$ manipulated boundary layer (actual u_τ); open symbols: LDV data from De Graaf & Eaton (2000) for a standard boundary layer.

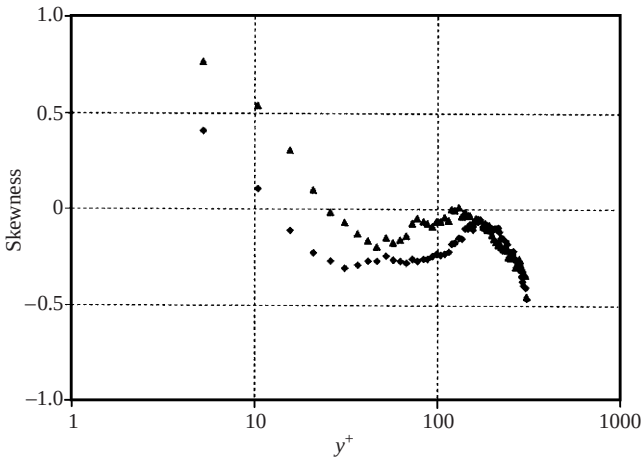

FIGURE 6. Skewness of the longitudinal velocity fluctuations profiles. Diamond: standard boundary layer; triangle: manipulated boundary layer.

reductions in both components of the velocity variance, longitudinal u'^2 and wall normal v'^2, are shown within the inner region. The maximum u'^2 and v'^2 reductions, located in the buffer region, are of the order of 30% and 40% respectively. Turbulence reduction is still evident when u'^2 and v'^2 are normalized with respect to the actual friction velocity.

The distribution of skewness and flatness of the longitudinal velocity fluctuations are shown in figures 6 and 7. Both the higher statistical moments of velocity seem to increase within the near-wall region. These increases in higher moments can also

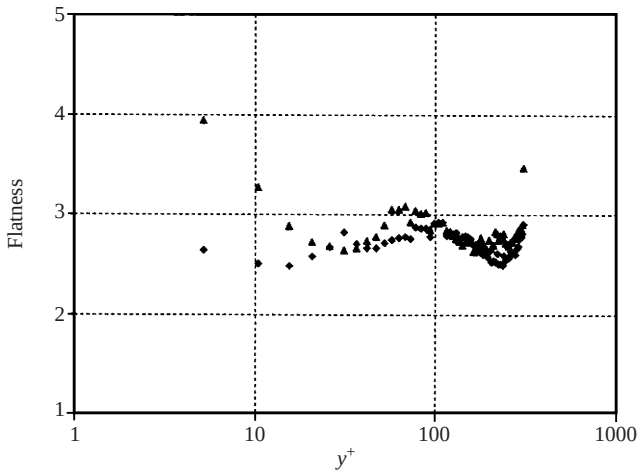

FIGURE 7. Flatness of the longitudinal velocity fluctuations profiles. Diamond: standard boundary layer; triangle: manipulated boundary layer.

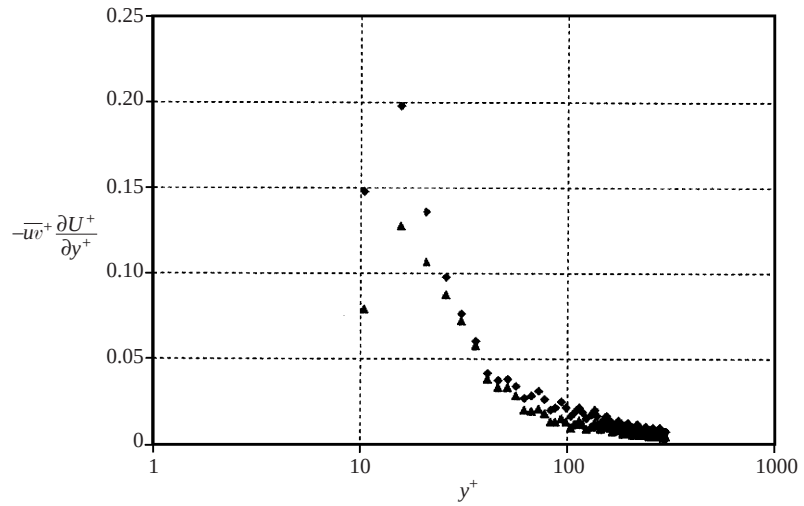

FIGURE 8. Turbulent kinetic energy production profiles. Diamond: standard boundary layer; triangle: manipulated boundary layer.

be interpreted as a manifestation of the increase in viscous sublayer thickness by the wall oscillation (Choi *et al.* 1998). Similar near-wall behaviour has been found by Baron & Quadrio (1996) and by Choi (1989) for the turbulent boundary layer over drag-reducing riblets.

The production of turbulent kinetic energy, whose instantaneous contribution is shown in figure 2, is displayed in figure 8 as a function of the distance from the wall. The result shows that wall oscillation reduces the peak of energy production in the buffer layer by about 35%.

In order to observe the overall structure of the flow, figures 9(*a*) and 9(*b*) display the double spatial correlation function, R_{uu}, for the streamwise fluctuating velocity in the plane $y^+ = 20$, parallel to the wall, respectively for the standard and manipulated boundary layers. Comparison between figure 9(*a*) and figure 9(*b*) shows similarities

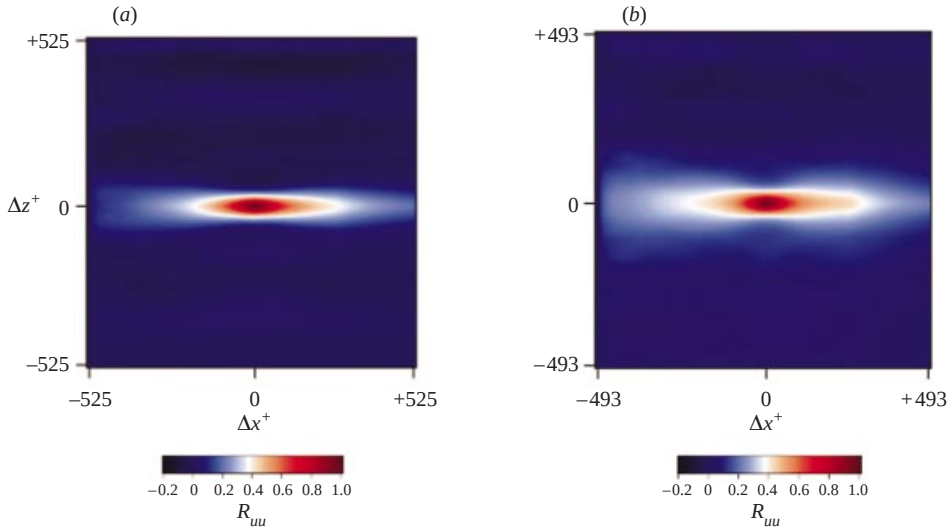

FIGURE 9. Double spatial correlation function R_{uu} in the plane $y^+ = 20$. (*a*) Natural boundary layer; (*b*) manipulated boundary layer.

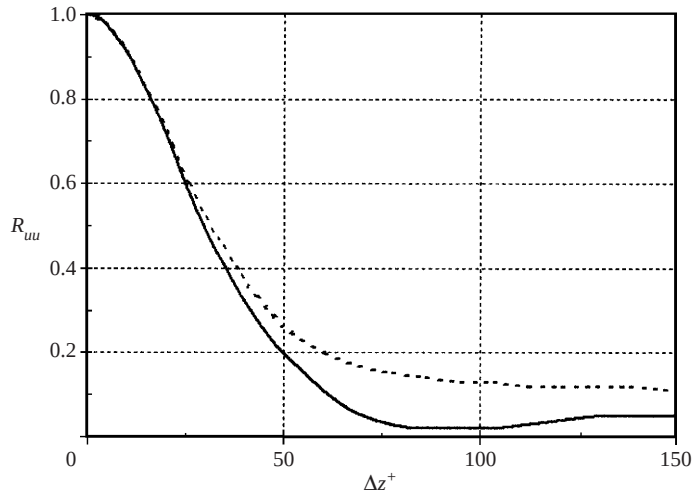

FIGURE 10. Spanwise correlation functions R_{uu} at $y^+ = 20$. Solid line: natural boundary layer; broken line: manipulated boundary layer.

between the two cases, which shows that, in spite of the great reduction in turbulence due to wall oscillation, the global organization of the flow is not qualitatively affected by the manipulation. Both correlograms exhibit an elliptical shape, because of the strong anisotropy between streamwise and spanwise directions. Nevertheless, from the quantitative analysis of the correlation functions and in particular of the spanwise ($\Delta x^+ = 0$) correlation reported in figure 10, a marked increase in the integral lateral scale (the area under the curves) produced by the wall oscillation clearly appears. This presumably means that the flow control increases the mean spacing of the low-speed streaks. A similar result is reported in Choi *et al.* (1998), where infrared images show that several low-speed streaks coalesce into a single streak as the wall oscillates, leading to the mean streak spacing increasing by about 45%, whereas the duration

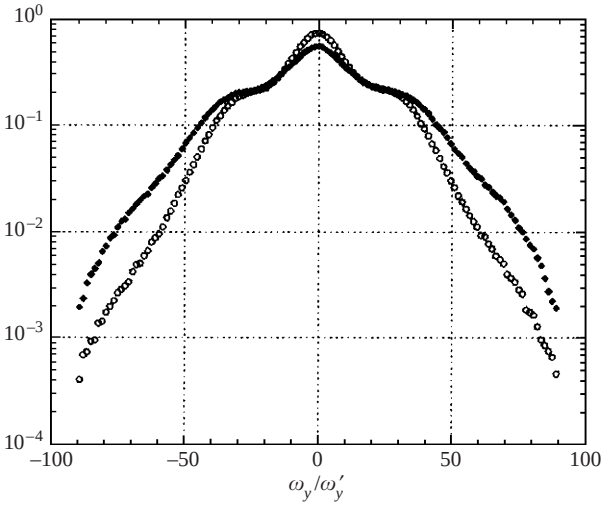

FIGURE 11. Probability density functions of ω_y at $y^+ = 20$. Solid diamond: natural boundary layer; open circle: manipulated boundary layer.

of the streaks $\mathscr{T}^+$ is multiplied by a factor 4 (Choi 2000). No information could be obtained from the present measurements about the low-speed longitudinal coherence, due to the fact that large scales are not resolved in the x-direction.

In order to gather information about the streak strength it is helpful to observe in figure 11 the probability density functions (PDF) of the normal fluctuating vorticity (see figure 1) ω_y, in planes $y^+ = 20$. In figure 11, ω_y is normalized with respect to the root-mean-square value of the natural flow vorticity, ω_y', at $y^+ = 20$. Comparison between the standard and the forced boundary layers shows that the PDF tails assume considerably lower values for the manipulated flow. This behaviour of the PDFs may be interpreted as the consequence of the weakening action of the wall oscillation on the velocity streaks. Jimenez & Pinelli (1999) showed by a numerical experiment that, by filtering the high values of ω_y flanking the low-speed streaks, a turbulent flow can be made to decay back to a laminar state. The present result experimentally confirms the association between the weakening of the velocity streaks, and therefore their stabilization (Schoppa & Hussain 2002), and the reductions in near-wall turbulence and skin friction.

The creation of internal inclined shear-layer structures (see figure 2) has historically been considered an important feature of the near-wall flow field (see e.g. Johansson *et al.* 1991). These shear layers are highly three-dimensional and inclined with respect to the wall and have been associated with instants of large turbulence production. In the present work, internal shear-layer motions were detected by applying the VISA technique (Kim 1985), which is the spatial counterpart of VITA technique (Blackwelder & Kaplan 1978; Blackwelder & Haritodinis 1983), widely used in hot-wire and LDV measurements. It is of interest to observe the effect of the manipulation on the spatial frequency of occurrence of internal shear-layer events n and on their structure. In figure 12 the non-dimensional frequency of occurrence of the events n^+, at $y^+ = 20$, as a function of the short integration length L^+ and of the threshold constant k is reported. The short integration length is scaled with respect to the standard boundary layer inner variables. The curves plotted in figure 12 show that, whatever the short integration length and the threshold constant, the number of

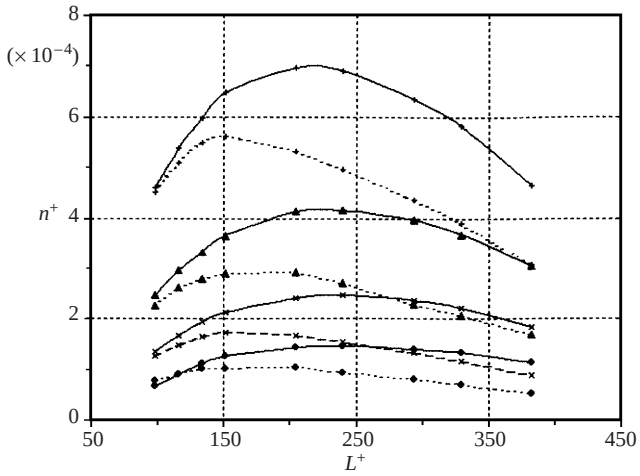

FIGURE 12. Frequency of occurrence of the VISA events, n^+ at $y^+ = 20$. Solid lines: natural boundary layer; broken lines: manipulated boundary layer. Plus: $k = 0.6$; solid triangle: $k = 0.8$; cross: $k = 1.0$; solid circle: $k = 1.2$.

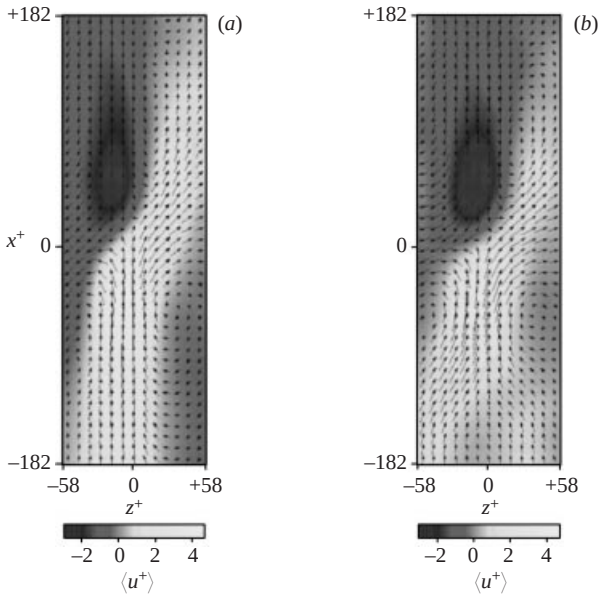

FIGURE 13. Conditionally ensemble-averaged VISA events at $y^+ = 20$. (a) Natural boundary layer; (b) manipulated boundary layer.

internal shear-layer events is reduced by the wall oscillation. Reduction in bursting frequency was also observed by Choi *et al.* (1998) and by Baron & Quadrio (1996). Moreover, the internal shear-layer event signatures in the plane $y^+ = 20$ have been conditionally ensemble averaged here, as described in Gottero & Onorato (2000), leading to the results shown in figures 13(a) and 13(b). Data in both plots were computed with the conditions $\mathrm{d}u/\mathrm{d}x < 0$ and $\mathrm{d}u/\mathrm{d}z > 0$. The VISA detection point, corresponding to the peak of the local variance, is at $x^+ = z^+ = 0$. The grey level maps highlight phase-averaged low-speed and high-speed streaks, normalized with respect

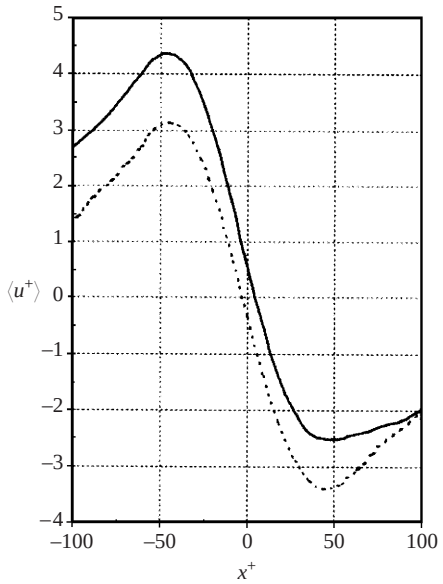

FIGURE 14. Conditionally ensemble-averaged VISA events at $y^+ = 20$. Solid line: natural boundary layer; broken line: manipulated boundary layer.

to the natural case; the vectors represent the phase-averaged fluctuating velocity field. In both flows the internal shear-layer event is at the border between a low- and a high-speed streak, where they show a kinked shape. The conditionally averaged fluctuating velocity field appears as if it were generated by two jets having opposite directions, strongly interacting in the internal shear-layer region. The conditional-averaged results in figure 13(b) show less definite contours of the velocity streaks. Quantitative differences between the basic and the manipulated boundary layers may be better appreciated in figure 14, obtained from figures 13(a) and 13(b) by making a vertical cut at $z^+ = 0$. The shear-layer structure appears slightly weaker for the manipulated boundary layer, but not enough to conclude that the motion amplitude is lower for the oscillating case (the observed reduction is of 5% only). Moreover the slope ($\mathrm{d}u^+/\mathrm{d}x^+$) has very similar values for the natural and the manipulated cases. On the other hand, figure 14 highlights a strong shift in the vertical direction, giving to a value of skewness (referring to the conditionally averaged results) close to zero for the manipulated flow, whereas it is positive for the standard boundary layer. This shifting may be due to the observed thickening of the near-wall viscous region. However, it should be noted that comparisons in figure 14 between the standard and the manipulated flows have been made at equal geometrical distance from the wall. As the value of u_τ is smaller for the manipulated flow, in terms of viscous lengths, the measurement plane is 'closer' to the wall. Measurements of Blackwelder & Kaplan (1978) show that the conditionally averaged VITA event at $y^+ = 20$ and at higher y^+ has a shape with positive skewness, whereas for smaller values of y^+ the conditionally averaged motion tends to be zero skewed.

In the previous section, Q2 motions were shown in planes (x, y) highlighting their spatial relationship with vortex signatures and with internal shear-layer motions. In particular, figure 2 refers to the contribution of Q2 motions to the generation of turbulent kinetic energy. It is also of interest to see how such motions are influenced by the wall oscillation. In figure 15 the number of Q2 events per unit length, N,

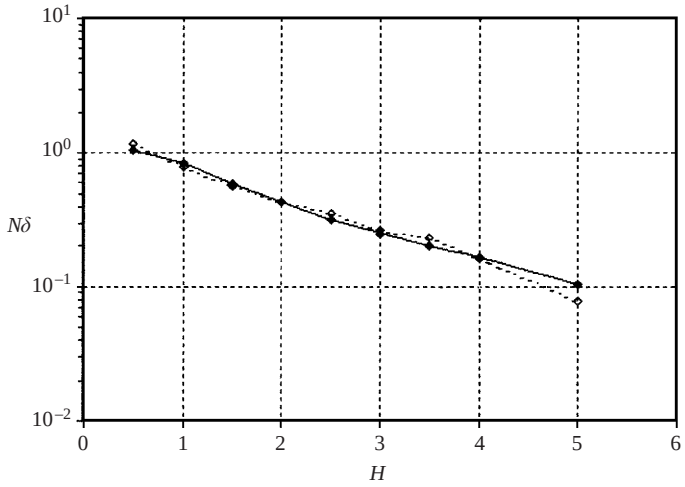

FIGURE 15. Frequency of Q2 events at $y^+ = 50$. Solid line: natural boundary layer; broken line: manipulated boundary layer.

at $y^+ = 50$, is displayed as a function of the threshold constant H. A Q2 event is detected when $|uv| > H(u'v')$ with $u < 0$ and $v > 0$ (Alfredsson & Johansson 1984), where u' and v' are the actual (corresponding to each case) r.m.s. values of the velocity fluctuations u and v. The two curves approximately coincide and have a linear behaviour as shown in Alfredsson & Johansson (1984), where analysis was also performed at $y^+ = 50$. Moreover, if the Q2 events were detected by using (for both the basic and the manipulated flow) the value of $(u'v')$ corresponding to the natural flow, the resulting number of events per unit length would be lower for forced flow, $(u'v')$ being reduced by about 25% (at $y^+ = 50$) by the wall oscillation.

5. Conclusions

PIV results in planes parallel to the wall in the buffer layer region are consistent with the conceptual model of mean near-wall structure proposed by Jeong *et al.* (1997). The analysis of images in planes normal to the wall reveals, in the logarithmic region of the boundary layer, a clear correspondence between the observed vortical structure organization and the packets of hairpin vortices observed by Adrian and coworkers (Adrian *et al.* 2000*a*, *b*).

Longitudinal and wall-normal turbulent velocity fluctuations as well as turbulent kinetic energy production are considerably reduced by wall oscillations; the amount of the reduction is comparable to numerical and experimental results from the literature.

The observed thickening of the viscous wall sublayer for the forced flow, evidenced by the upward shifting of the logarithmic velocity profile and by the skewness and flatness behaviour near the wall, reflects a clear reorganization of the near-wall turbulent structures, involving presumably an increase in the small eddies scale and a displacement of the turbulent events outwards from the wall.

The spanwise integral length scale is increased by the manipulation; this may reflect an increase of the low-speed streak spacing, presumably due to the enhanced mixing near the wall caused by the presence of oscillating Stokes layers. These transversally oscillating layers, besides being the cause of the mean velocity gradient reduction at the wall (according to Choi *et al.* 1998), may induce continuous shifting of the

near-wall longitudinal vortices relative to the velocity streaks, thus weakening the low-speed streaks. This is highlighted by the reduction in the high value range of the wall-normal vorticity in the manipulated case and confirms the association between the weakening of the velocity structures and the reduction of the near-wall turbulence activity.

The weakening of the velocity streaks is also proved by the observed attenuation of the wall events activity, as the manipulated flow is characterized by the occurrence of fewer internal shear-layer events and by slightly lower amplitude of the conditionally averaged high values of $\mathrm{d}u/\mathrm{d}x$, detected by VISA technique. Also, the second quadrant motion events, for the manipulated flow, are less frequent and less intense. This result may be directly related to the reduction of existing trains of vortical structures.

As a final conclusion, the main results in this investigation are consistent with the scenario in which the oscillating transversal layers weaken the wall velocity streaky structures. As a consequence, the streaky structures become more stable causing the attenuation of the regeneration mechanisms of the longitudinal streamwise vortices (see Schoppa & Hussain 2002) and then the reduction of the wall turbulence activities.

The authors wish to thank Mr Dario Caiero, student, for his help in taking the measurements. This work was supported by grants from the CNR and MURST.

REFERENCES

Adrian, R. J. 1991 Particle-imaging techniques for experimental fluid mechanics. *Annu. Rev. Fluid Mech.* **23**, 261–304.

Adrian, R. J., Christiansen, K. T. & Liu, Z. C. 2000*a* Analysis and interpretation of instantaneous turbulent velocity fields. *Exps. Fluids* **29**, 275–290.

Adrian, R. J., Meinhart, C. D. & Tomkins, C. D. 2000*b* Vortex organization in the outer region of the turbulent boundary layer. *J. Fluid Mech.* **422**, 1–54.

Alfredsson, P. H. & Johansson, A. V. 1984 On the detection of turbulence-generating events. *J. Fluid Mech.* **139**, 325–345.

Baron, A. & Quadrio, M. 1996 Turbulent drag reduction by spanwise wall oscillations. *Appl. Sci. Res.* **55**, 311–326.

Blackwelder, R. & Eckelmann, H. 1979 Streamwise vortices associated with the bursting phenomenon. *J. Fluid Mech.* **94**, 577–594.

Blackwelder, R. & Kaplan, R. E. 1978 On the wall structure of turbulent boundary layers. *J. Fluid Mech.* **76**, 89–112.

Blackwelder, R. F. & Haritodinis, J. H. 1983 Scaling of the bursting frequency in turbulent boundary layers. *J. Fluid Mech.* **132**, 87–103.

Choi, K. S. 1989 Near wall structure of turbulent boundary layer with riblets. *J. Fluid Mech.* **208**, 417–458.

Choi, K. S. 2000 European drag reduction – research recent developments and current status. *Fluid Dyn. Res.* **26**(5), 325–335.

Choi, K. S., DeBisschop, J. R. & Clayton, B. R. 1998 Turbulent boundary layer control by means of spanwise wall oscillations. *AIAA J.* **36**(7), 1157–1163.

Chong, M. S., Perry, A. E. & Cantwell, B. J. 1990 A general classification of three-dimensional flow fields. *Phys. Fluids* A **2**, 765–777.

De Graaf, D. B. & Eaton, J. K. 2000 Reynolds-number scaling of the flat-plate turbulent boundary layer. *J. Fluid Mech.* **422**, 319–346.

Dhanak, M. B. & Si, C. 1999 On reduction of turbulent wall friction through spanwise wall oscillations. *J. Fluid Mech.* **383**, 175–195.

Di Cicca, G. M. 2001 Experimental study of wall turbulent flows and their control. PhD thesis, Politecnico di Torino.

Di Cicca, G. M., Onorato, M., Iuso, G., Bollito, A. & Spazzini, P. G. 1999 DPIV study of a non

canonical boundary layer flow. In *Proc. of the 3rd Intl Workshop in Particle Image Velocimetry*. Santa Barbara, CA, USA.

Di Cicca, G. M., Onorato, M., Iuso, G. & Spazzini, P. G. 2001 Application of particle image velocimetry to wall turbulence studies. *Atti dell'Accademia delle Scienze di Torino* **135**.

Gottero, M. & Onorato, M. 2000 Low-speed streak and internal shear layer motions in a turbulent boundary layer. *Eur. J. Mech. B – Fluids* **19**, 23–36.

Iuso, G. & Onorato, M. 1995 Turbulent boundary layer manipulation by outer layer devices. *Meccanica* **30**(4), 359–376.

Iuso, G., Onorato, M., Spazzini, P. G. & Di Cicca, G. M. 2002 Wall turbulence control by large scale streamwise vortices. *J. Fluid Mech.* (in press).

Jeong, J., Hussain, F., Schoppa, W. & Kim, J. 1997 Coherent structures near the wall in a turbulent channel flow. *J. Fluid Mech.* **332**, 185–214.

Jimenez, J. & Moin, P. 1991 The minimal flow unit in near wall turbulence. *J. Fluid Mech.* **225**, 221–240.

Jimenez, J. & Pinelli, A. 1999 The autonomous cycle of near-wall turbulence. *J. Fluid Mech.* **389**, 335–359.

Johansson, A. V., Alfredsson, P. H. & Kim, J. 1991 Evolution and dynamics of shear layer structures in near-wall turbulence. *J. Fluid Mech.* **224**, 579–599.

Jung, W. J., Mangiavacchi, N. & Akhavan, R. 1992 Suppression of turbulence in wall-bounded flows by high-frequency spanwise oscillations. *Phys. Fluids* A **4**(8), 1605–1607.

Kim, J. 1985 Turbulence structures associated with the bursting event. *Phys. Fluids* **28**(1), 52–58.

Laadhari, F., Skandaji, L. & Morel, R. 1994 Turbulence reduction in a boundary layer by a local spanwise oscillating surface. *Phys. Fluids* **6**(10), 3218–3220.

Landahl, M. T. 1990 On the sublayer streaks. *J. Fluid Mech.* **212**, 593–614.

Onorato, M., Iuso, G., Di Cicca, G. M. & Spazzini, P. G. 2000 Turbulence control in near wall flows. In *AIAA Fluids 2000 Conference (Paper AIAA-2000-2659)*. Denver, Co., USA.

Panton, R. L., ed. 1997 *Self-sustaining mechanisms of wall turbulence, advances in fluid mechanics*, vol. 15. Southhampton, UK: Computational Mechanics Publications.

Robinson, S. K. 1991 Coherent motions in the turbulent boundary layer. *Annu. Rev. Fluid Mech.* **23**, 601–639.

Robinson, S. K. 1993 The kinematics of turbulent boundary layer structures. TM 103859. NASA.

Scarano, F. & Riethmuller, M. L. 1999 Iterative multigrid approach in PIV image processing with discrete window offset. *Exps. Fluids* **26**, 513–523.

Schoppa, W. & Hussain, F. 2002 Coherent structure generation in near-wall turbulence. *J. Fluid Mech.* **453**, 57–108.

Smith, C. R. & Metzler, S. P. 1983 The characteristics of low-speed streaks in the near-wall region of a turbulent boundary layer. *J. Fluid Mech.* **129**, 27–54.

Willert, C. E. & Gharib, M. 1993 *Digital particle image velocimetry. Theory and applications.* Delft, Germany: Delft University Press.

Zhou, J., Adrian, R. J., Balachandar, S. & Kendall, T. M. 1999 Mechanisms for generating coherent packets of hairpin vortices in channel flow. *J. Fluid Mech.* **387**, 353–396.